Earthquakes and Structures, *Vol. 27, No. 1 (2024) 69-82*
https://doi.org/10.12989/eas.2024.27.1.069

Seismic performance enhancement of a PCI-girder bridge pier with shear panel damper plus gap: Numerical simulation

Andika M. Emilidardi[a], Ali Awaludin*, Andreas Triwiyono[b], Angga F. Setiawan[c], Iman Satyarno[d] and Alvin K. Santoso[e]

Department of Civil and Envinromental Engineering, Universitas Gadjah Mada, Grafika Street 2, Sleman, Special Region of Yogyakarta, Republic of Indonesia

(Received August 23, 2023, Revised August 24, 2023, Accepted May 3, 2024)

Abstract. In the conventional seismic design approach for a bridge pier, the function of the stopper, and shear key are to serve as mechanisms for unseating prevention devices that retain and transmit the lateral load to the pier under strong earthquakes. This frequently inflicts immense shear forces and bending moments concentrated at the plastic hinge zone. In this study, a shear panel damper plus gap (SPDG) is proposed as a low-cost alternative with high energy dissipation capacity to improve the seismic performance of the pier. Therefore, this study aimed to investigate the seismic performance of the pre-stressed concrete I girder (PCI-girder) bridge equipped with SPDG. The bridge structure was analyzed using nonlinear time history analysis with seven-scaled ground motion records using the guidelines of ASCE 7-10 standard. Consequently, the implementation of SPDG technology on the bridge system yielded a notable decrease in maximum displacement by 41.49% and a reduction in earthquake input energy by 51.05% in comparison to the traditional system. This indicates that the presence of SPDG was able to enhance the seismic performance of the existing conventional bridge structure, enabling an improvement from a collapse prevention (CP) level to an immediate occupancy (IO).

Keywords: energy dissipation; plastic hinge; seismic performance; shear panel damper plus gap; structural response

1. Introduction

Powerful earthquakes have the potential to cause catastrophic damage to bridges, and one of these damages is the unseating of the superstructure. The failure of unseating potentially occurs when bridge girders are supported by elastomeric rubber bearings (ERB) due to limited deformation and low energy dissipation capacities (Abdel Raheem 2009, Yenidogan *et al*. 2021). This failure occurs when the lateral deformation exceeds the deformation limit, which is indicated by sliding (Abdel Raheem 2009, Mosalam *et al*. 2015, Xiang *et al.* 2021, Yao *et al.* 2021). A viable solution for averting the issue of unseating involves the installation of a stopper between two spans, accompanied by shear keys. This combined approach serves to effectively maintain the lateral deformation of the superstructure that arises due to the forces exerted by earthquake loads (Mosalam *et al*. 2015, Setiawan and Takahashi 2018). However, the inclusion of the stopper and shear key within the bridge structure triggers the creation of plastic hinges at the lower part of the pier (Moehle and Eberhard 2000), indicating that a large amount of earthquake energy is absorbed by the pier. In this scenario, the greater the energy absorbed, the more pronounced the potential for extensive damage at the piers when the earthquake forces surpass the plastic hinge's capacity (Moehle and Eberhard 2000). In order to reduce pier damage, one of the conventional methods is to increase the cross-sectional area of the pier or design the pier using a small response modification factor (R). One solution to prevent bridge pier damage is to increase the energy dissipation capacity of the structure using lead rubber bearings (LRB), high-damping bearings (HDB), friction pendulum bearings (FPB), and metallic yield dampers (Becker and Mahin 2012, Shoaei *et al*. 2018, Wang *et al*. 2021, Xu *et al*. 2021, Zhang *et al*. 2023). Another way to enhance the structure's ability to reduce vibration and prevent structural damage is by implementing tuned mass dampers, which can enhance the seismic performance of structures by increasing the damping coefficient of reinforced concrete structures (Cao and Li 2022, Li *et al*. 2023, Chen *et al*. 2023). Metallic yield dampers have advantages over other passive control devices due to their simple system and cost-effective, requiring less design and manufacturing effort compared with popular isolation systems such as LRB, HDB, and FPB (Xiang *et al.* 2019).

Metallic yield dampers have been widely developed in

*Corresponding author, Associate Professor
E-mail: ali.awaludin@ugm.ac.id
[a]Master Student
E-mail: andika.emilidardi@mail.ugm.ac.id
[b]Professor
E-mail: andreas.triwiyono@ugm.ac.id
[c]Assistant Professor
E-mail: angga.fajar.s@ugm.ac.id
[d]Professor
E-mail: imansatyarno@ugm.ac.id
[e]Master Student
E-mail: alvinkurniawansantoso@mail.ugm.ac.id

http://www.techno-press.com/journals/eas&subpage=7
ISSN: 2092-7614 (Print), 2092-7622 (Online)

reinforced concrete structures to improve the dissipation capability of buildings or bridges (Chen *et al*. 2007, Najari Varzaneh and Hosseini 2019, Ying *et al*. 2020, Wu *et al*. 2022). Based on previous studies, it has been observed that including a metallic damper in building structures can enhance structural stiffness, strength, and energy dissipation (Shi *et al*. 2018, Han *et al*. 2019, Ren *et al*. 2021). This improvement decreases structural response, thereby mitigating damage to the main structural elements during seismic excitation. To enhance the seismic performance of highway bridges supported by laminated rubber bearings, the suggestion was made to utilize yielding steel dampers instead of other passive control device and traditional shear keys as restraining mechanisms for the bearings. A shear panel damper (SPD) is a metallic yield damper developed as a passive control device for the bridge structure and aims to replace the conventional system equipped with stoppers and shear keys (Setiawan and Takahashi, 2018). In terms of its application method, practically, this device is easy to replace without lifting the superstructure since it is not directly connected to the superstructure. The implementation of (SPD) technology within the bridge structure should be accompanied by the inclusion of a gap, referred to as a shear panel damper plus gap (SPDG). This addition serves the purpose of preventing SPD from engaging under traffic traction eliminating fatigue, and maintaining its performance. In a study by Haroki *et al*. (2023), implementing SPDG on slab-on-pile bridges showed a satisfying result where it could improve the seismic performance under the Yogyakarta site. Meanwhile, Santoso *et al*. (2023) compared the seismic performance of a box girder bridge equipped with SPDG and the existing bridge equipped with lead rubber bearing (LRB) in Makassar (Santoso *et al*. 2023). As a result, SPDG showed comparable results to LRB, where the bridge performance for both models was at the operational limit state. However, the maximum ground acceleration in Makassar, which was only 0.5 g, was weaker than in Yogyakarta, which was 0.9 g. Based on a previous study, the implementation of SPDG on PCI-girder bridge structures has not been conducted yet. Currently, PCI-girder is one of the most common bridges that is widely used (Bhavani *et al*. 2018). According to the study by Vishal *et al*. (2014), Aishwarya *et al* (2019) PCI-girder has a large superstructure self-weight in its superstructures, leading to high risk of the earthquake demand for this bridge system. Therefore, further study needs to be conducted to determine SPDG's effect on the pier bridge structure under a severe earthquake.

The main objective of this study was to investigate the seismic performance of the PCI-girder bridge pier model equipped with SPDG, in response to scaled ground motion records that account for the Yogyakarta site. To achieve this objective, the initial step involved conducting an elastic analysis to design the equipped bridge system. Subsequently, the nonlinear time history analysis was conducted to observe dynamic responses as well as the seismic performance of the bridge. The findings of this study were compared across two varying scenarios of bridge structures, which include those equipped with SPDG devices and those without. This comparison served as a means to underscore the enhanced seismic performance resulting from the inclusion of SPDG technology.

2. Analysis method

In this study, two numerical models of the Yogyakarta International Airport (YIA) railway bridge were investigated namely Models A and B. Model A was an existing bridge equipped with elastomeric rubber bearing (ERB), while Model B was the proposed bridge equipped with SPDG. Both models were bolstered by elastic springs, serving as representative elements to simulate the interaction between the soil and the piles of the bridge under investigation and were calculated based on the code provision AASHTO LFRD 2017 (AASHTO 2017), ASCE 41-17 (ASCE 2017), and *Analytical and Computer Methods in Foundation Engineering* (Bowles 1974). Furthermore, the dimensions and parameters of each structural element were determined based on the detailed engineering design (DED) of the YIA railway bridge. The analysis procedure was divided into two sections, which include the elastic and nonlinear time history analyses.

2.1 Elastic design procedure of SPDG

In a broader context, the bridge structures were simplified to include only mass and stiffness characteristics, as they were assumed to exhibit elastic behavior in response to seismic forces. The pier mass was assumed to lump at the top pier, which comprises the mass of the superstructure along the tributary area, the pier head mass, and one-half of the top pier mass. Model A was equipped with shear keys and stoppers as lateral restraints, which were rigidly connected to the pier to ensure the substructure stiffness was properly represented by the pier. Meanwhile, the ERB and SPDG provided a low lateral stiffness that was calculated manually according to the code provision AASHTO LRFD 2017 and the previously reviewed studies (Sabouri-Ghomi *et al*. 2005, Chen *et al*. 2007). The study assumed that the initial stiffness of ERB and the effective stiffness of SPDG functioned in a parallel arrangement, while both were connected in series with the elastic stiffness of the pier. Furthermore, in Model B, the ERB linked the girder and the pier head, while the SPDG was positioned on the pier head without a direct connection to the girder. This arrangement was intended to prevent the SPDG from opposing vertical forces, as shown in Fig. 3. The force-displacement concept of SPDG is illustrated, as shown in Fig. 1. In this concept, the presence of a gap influenced the hysteresis response of SPD by introducing an initial displacement with zero stiffness along the gap length (Sabouri-Ghomi *et al*. 2005, Setiawan and Takahashi 2018, Jiang *et al*. 2019).

The analysis of the structure of a PCI-girder bridge equipped with SPDG initially started by calculating the substructure capacity as a benchmark parameter for SPDG design. The bridge pier was then analyzed based on AAHSTO LFRD 2017 to determine its flexural and shear capacity, which was defined as V_p. The SPDG dimensions

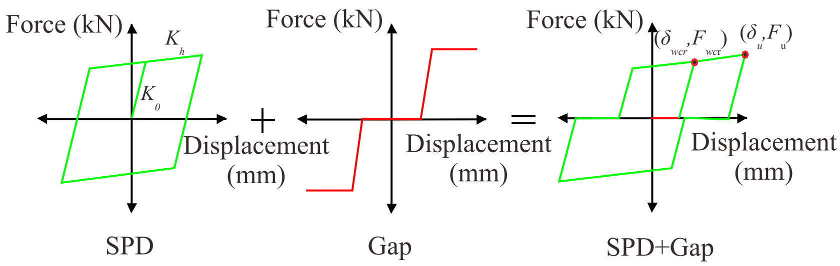

Fig. 1 The SPDG with a gap concept

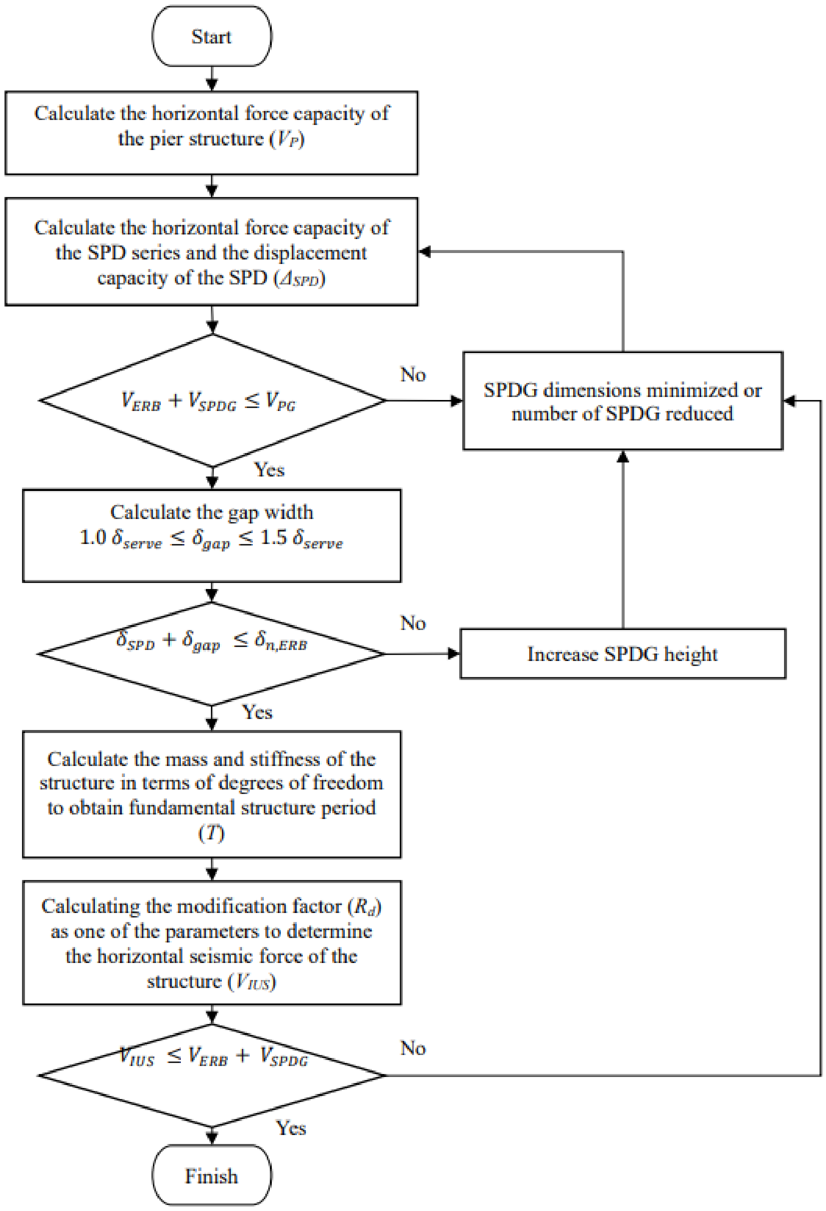

Fig. 2 Procedure for design SPDG as bridge restraining devices

were designed to ensure that the horizontal ultimate capacity value of the SPDG and ERB series did not exceed V_p. This was done to prevent damage to the pier, as demonstrated in the Santoso *et al*. (2023). In addition, parameters that were needed to develop the hysteresis model of the SPDG were horizontal stiffness (K_0), post-yield stiffness (K_h), effective stiffness (K_{ef}), yield force of the SPDG web (F_{wcr}), and the ultimate force of the SPDG web (F_u). The ultimate shear strain (γ_u) was delivered from the SPDG deformation limit for about 16%-20% of the SPDG height (h_w) Jing *et al*. 2019, Liu *et al*. 2013. The yield force of the web (F_{wcr}) was obtained from the multiplication of τ_{wcr}, web-thickness (t_w), and web-wide (b_w). The ultimate force of the web (F_u) also was obtained

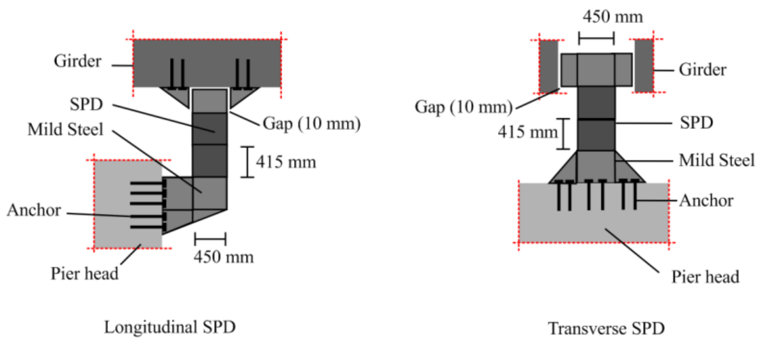

Fig. 3 Proposed SPDG device in longitudinal and transverse directions

from the multiplication of ultimate shear stress (τ_u), web-thickness (t_w), and web-wide (b_w), where ultimate shear stress of the web was expressed in Eq. (10). While τ_u is obtained from the sum of the ultimate shear stress of the flange (τ_f) and the ultimate shear stress of the web (τ_w) as expressed in Eqs. (9)-(11). Then, the SPD gap should be larger than the service load displacement and should not exceed 1.5 service load displacements. This ensures that the sum of the SPD displacement and the gap displacement did not exceed the ERB displacement.

$$K_0 = \frac{F_{wcr}}{\delta_{wcr}} \tag{1}$$

$$K_h = \frac{F_u - F_{wcr}}{\delta_u - \delta_{wcr}} \tag{2}$$

$$K_{ef} = \frac{F_u}{\delta_u} \tag{3}$$

$$F_{wcr} = \tau_{wcr} b_w t_w \tag{4}$$

$$F_u = \tau_u b_w t_w \tag{5}$$

$$\delta_{wcr} = \gamma_{wcr} b_w \tag{6}$$

$$\delta_u = \gamma_u b_w \tag{7}$$

$$\tau_u = \tau_f + \tau_w \tag{8}$$

$$\tau_f = 0.00287 \frac{b_f}{b_w} \frac{t_f}{t_w} \left(\frac{t_f}{t_w} 4 \frac{h_w}{(n_L+1) R_w b_w} + 2 \right) T_{fcr} \tag{9}$$

$$\tau_w = \left(0.918 + \frac{0.038}{{R_w}^2} + 2\right) T_{wcr}; \left(0.918 + \frac{0.038}{{R_w}^2} + 2\right) \leq 1.2 \tag{10}$$

$$\tau_w = 1.2 \tau_{wcr}; \left(0.918 + \frac{0.038}{{R_w}^2} + 2\right) > 1.2 \tag{11}$$

In Model A, the displacement modification factor (R_d) was obtained from the seismic design of the railway bridge, following SNI 2833:2016 (Badan Standardisasi Nasional Indonesia, 2016). However, the influence of implementing SPDG on the bridge system could increase the fundamental period (Santoso *et al.* 2023). Based on these findings, the displacement modification factor for Model B was calculated using Eq. (12) (AASHTO 2011). This modification factor, R_d, was obtained by calculating the maximum ductility of the SPDG (μ_D), the characteristics of the ground motions period (T^*), which was $1.25T_s$, and the fundamental structure period (T).

$$R_d = \left(1 - \frac{1}{\mu_D}\right) \frac{T^*}{T} + \frac{1}{\mu_D} \tag{12}$$

The fundamental period of the bridge served as a key parameter for acquiring the spectral acceleration, which was achieved through its representation on the designed response spectrum through plotting. Subsequently, the demand earthquake force was obtained by multiplying the elastic earthquake coefficient and the structural weight, divided by the response modification factor (R_d). The demand force was used to ensure that the shear strength capacity of the pier satisfied the design provision. In this study, an R_d-value of 1.5 was applied for the pier, given that the bridge was categorized as an essential structure. However, the R_d-values of the superstructure for Models A and B were 1.5 and 1.75, respectively. The detailed design flowchart of SPDG on PCI-girder bridge structure is shown in Fig. 2.

The SPDG's total yield strength was determined based on the elastic design concept, in which could be represented based on the ratio between the total yield strength of SPDG to the pier. The low ratio might affect the early yield on the damper, resulting to the ineffective energy dissipation capability during strong earthquake events. Otherwise, when the ratio was too high, the yielding phase of the damper might be difficult to achieve, resulting in the greater ultimate strength capacity of SPDG to the pier. SPDG as damper and stopper was designed to have a yield strength of 50% of the pier capacity. This was a reference to the study of Hube and Rubilar (2015), which explained that the shear key or stopper element should be half of the pier capacity. Meanwhile, Santoso *et al.* (2023) proposed the ratio in the range of 0.53 - 0.73 corresponding to an operational limit state or the equivalent of minor damage, as defined by NCHRP (2013). Furthermore, the SPDGs used had a 415×450 mm^2 dimension with a gap of 10 mm, as shown in Fig. 3. The arrangement of these SPDGs included 12 in the longitudinal direction and 14 in the transverse direction on a single pier. Each SPDG possessed a maximum strength capacity of 15939.4 kN, while the elastic capacity of the pier amounted to 31859.8 kN.

2.2 Bridge model description for nonlinear time history analysis

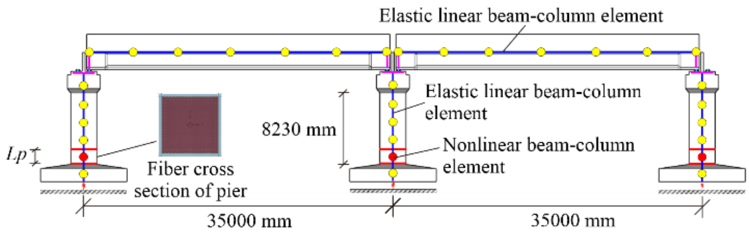

Fig. 4 Longitudinal view of the bridge model

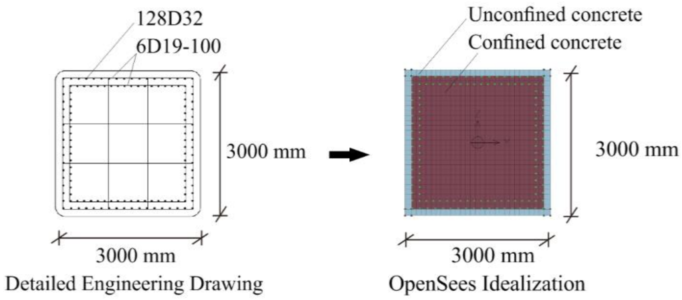

Fig. 5 The pier section and its idealization in OpenSees

Table 1 Concrete material properties

Concrete	e_{psc0}	f_{pc} (MPa)	e_{pshU}	f_{pcu} (MPa)	λ	f_t (MPa)	E_{ts} (MPa)
Unconfined	0.002	33.20	0.0041	6.64	0.10	3.59	33200
Confined	0.0022	36.84	0.060	7.37	0.10	3.78	36839.91

In this study, A two-span, simply supported PCI-girder bridge model was investigated using nonlinear time history analysis, as shown in Fig. 4. This analysis adhered to the model idealization previously undertaken by (Guo *et al.* 2019, Xiang *et al.* 2019, Suarjana *et al.* 2020, Farahpour and Hejazi 2023). Superstructure loads were evenly distributed on the superstructure element to load the bridge pier underneath. The model was limited to only two-span of the actual structure, so the point load has been implemented on the side of the pier to represent the superstructure load where the girder was not modeled. Furthermore, the mass of the superstructure was assumed to lump at each node along the girder, which had a length of 35 m and was divided into six elements. Each girder was supported by ERB, which linked the girder to the substructure. The pier had a height of 8.23 m with a 3×3 m^2 column dimension. Model A was outfitted with lateral restraints in the form of a stopper and shear key, both of which were installed on the pier head, while the SPDG incorporated in Model B provided lateral restraint and energy dissipation capacity.

The bridge model was created using Open System for Earthquake Engineering Simulation (OpenSees). During this simulation, all parts of the superstructures, pier head, and pile cap were modeled as elastic sections with force-based beam-column elements. Particularly, the pier was defined as a fiber section along the plastic hinge length (L_p) of 932.96 mm, which was calculated using Eq. (13) (AASHTO 2011, Yuan *et al.* 2017, Kurniawan Santoso *et al.* 2022), where L_p is the plastic hinge length, L represents the pier height, f_{ye} denote the yield strength of the longitudinal reinforcing steel, and d_{bl} is the diameter of the steel. In the OpenSees, the pier was idealized using the Hinge-Radau integration rule. This entailed the application of a fiber and an elastic section solely along and at the outer part of the plastic hinge zone respectively (Suarjana *et al.* 2020, Kurniawan Santoso *et al.* 2022). To represent the nonlinear material effect, the pier-fiber sections were defined into unconfined and confined concretes, and the reinforcement was carried out using steel materials, as shown in Fig. 5. In response to a large deformation effect due to the gravity load, the analysis also incorporated P-Δ with large displacement or corotational effects.

$$L_p = 0.08L + 0.022 f_{ye} d_{bl} \geq 0.044 f_{ye} d_{bl} \tag{13}$$

In accordance with several previous studies, the concrete material was modeled using the Concrete02 approach (Kent and Park 1971, Filippou *et al.* 1983, Filippou and Mazzoni 2010). Furthermore, the concrete parameters considered were its compressive strength (f_{pc}), crushing strength (f_{pcu}), strain at maximum strength (e_{psc0}), strain at crush (e_{pshU}), the ratio between unloading and initial slope (λ), tensile strength (f_t), and tensile softening stiffness (E_{ts}), shown in Table 1.

Meanwhile, the reinforcing steel was idealized as a reinforcing material in OpenSees (Mohle and Kunnath 2012), with a *MinMax* material serving as the maximum strain. Accordingly, the input material for reinforcing steel was yield stress (f_y), ultimate stress (f_u), initial elastic tangent (E_s), tangent at initial strain hardening (E_{sh}), strain corresponding to initial strain hardening (e_{sh}), strain at peak stress (e_{ult}), and maximum strain (ε_{min} and ε_{max}), as summarized in Table 2.

Table 2 Reinforcing steel material properties

f_y (MPa)	F_u (MPa)	E_s (MPa)	E_{sh} (MPa)	e_{sh}	e_{ult}	ε_{min}	ε_{max}
390	505	200000	2000	0.02	0.22	-0.26	0.26

Table 3 SPDG and ERB material properties

Component	f_y (kN)	K_0 (kN/mm)	b	K_v (kN/mm)	Max horizontal displacement (mm)
SPDG	893.22	692.31	0.003	3903.61	132.80
ERB	406.86	2.65	-	5520833.33	153.60

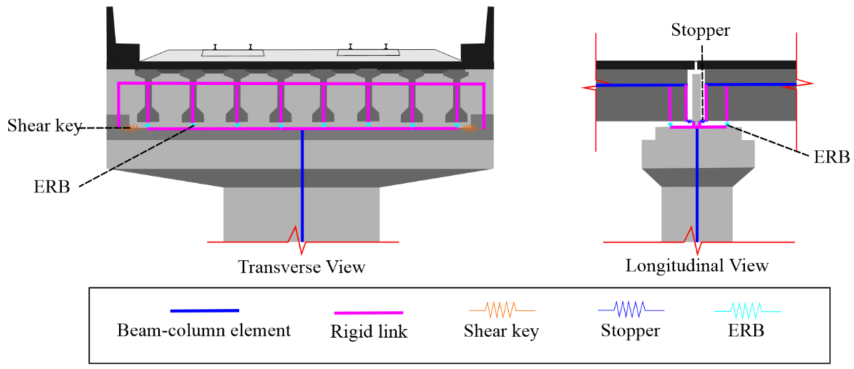

Fig. 6 Idealization of the structure system for Model A

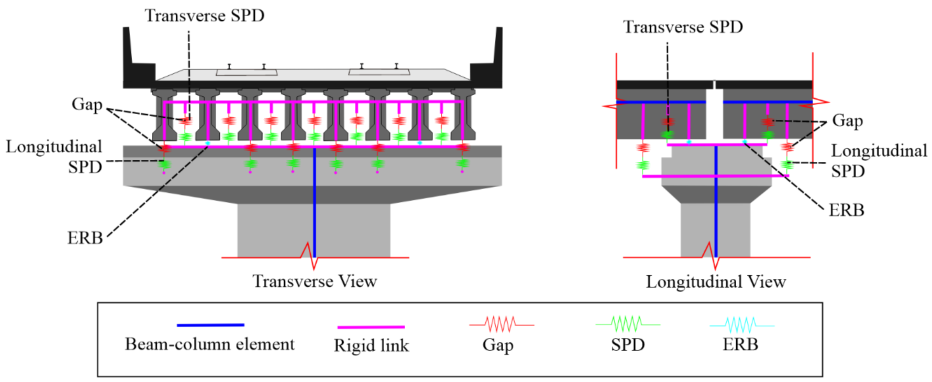

Fig. 7 Idealization of the structure system for Model B

Several components, such as the shear key, stopper, and rigid arm, were modeled using zero-length elements. The rigid arm was a connection between link-to-link or link-to-element that was assumed to be perfectly rigid with an elastic stiffness of 10^{15} N/mm. Meanwhile, the shear key and stopper were modeled using elastic-perfectly plastic material to represent the pounding behavior that occurred after the deformation of the superstructure exceeded the gap length. According to a study conducted by Megally (2001) indicated that the impact force on the shear key or stopper element was relatively small. Furthermore, Bi and Hao (2015) posited that the dynamic amplification factor on the shear key could be neglected when the ratio of pulse duration to the natural period of the system was large. In this study, the ratio between pulse duration and natural period of the system was 51.73 s and 8.33 s for Model A and Model B, respectively. In addition, the small gap, which was up to 20 mm, resulted in a reduced impact effect on the shear key or stopper element (Jankowski *et al*. 2000). In this model, the SPDG, which also functioned as a shear key, had a gap of 10 mm. Thus, the impact force effect on the shear key, stopper, and SPDG was not included in this model. In Model A, a gap length of 100 mm and 35 mm were used in the stopper and shear key, respectively. For Model B, a gap length of 10 mm was intentionally designed to prevent the dissipation of energy by the SPDG during service conditions. The two-node link element was also used to idealize ERB, SPDG, and the foundation system. Accordingly, the SPDG material was idealized using *steel01* (Filippou and Mazzoni 2012), while ERB was idealized as an elastic-bilinear model. The input material in this process involves yield strength (f_y), initial elastic tangent (K_0), the strain-hardening ratio between the post-yield tangent, and the initial tangent (b), as presented in Table 3. The arrangement of the bearing-damper bridge system for Models A and B is shown in Figs. 6 and 7, respectively. Furthermore, the pile foundations were simulated as a linear spring, with the assumption of representing a flexible soil

Table 4 Selected ground motions

No.	Earthquake	Fault	*Mw*	*R* (km)	V_{30} (m/s)	Scale Factor (*SF*)	
						SF_x	SF_y
1	Kobe-1104	Strike-slip	6.9	17.85	256	2.7	2.5
2	Darfield	Strike-slip	7.0	17.64	204	2.15	2.7
3	Kobe-1116	Strike-slip	6.9	19.14	256	2.15	2.4
4	Superstition Hill 02	Strike-slip	6.54	17.03	208.71	5.2	5.1
5	Tottori	Strike-slip	6.61	16.60	138.76	2.68	3.7
6	Northern Calif	Strike-slip	6.5	26.72	219.31	2.8	2.81
7	Imperial Valley	Strike-slip	6.53	19.76	471.53	2.32	2.2

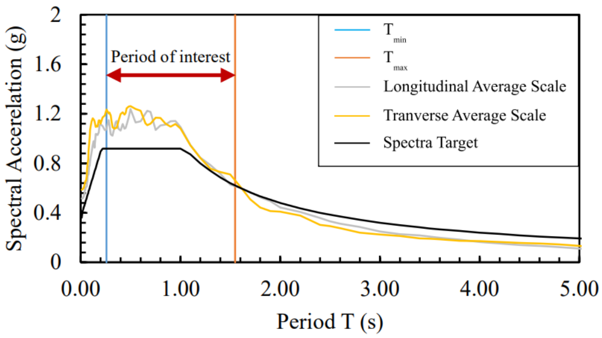

Fig. 8 The scaled response spectrum in longitudinal and transverse directions

and a fixed constraint (ASCE 2017, Bowles 1974). In this regard, the parameters considered include pile group vertical stiffness (K_{sv}) and pile group rotational stiffness (K_{sr}). The results of this study comprised seismic performance evaluation and the proportion of earthquake input energy. Accordingly, the seismic performance was investigated by observing the maximum drift ratio due to the designed earthquakes. Because the focus was on pier performance, the primary observation involved obtaining the skeleton curve through pushover analysis conducted exclusively on the substructure (i.e., pier and foundation). Furthermore, the performance level of each model was compared to the structural performance level standards outlined in ASCE 41-17 and FEMA-356 (ASCE 2017, ASCE 2000). An input energy analysis was conducted to examine the proportion of energy dissipation by the SPDG in mitigating seismic excitation. As outlined by Dindar *et al.* (2014), ground shaking transmits earthquake energy to the structure, referred to as input energy. In this context, the energy of the structure should ideally equate to the input energy. The structure energy comprised kinetic energy (E_K), viscous damping energy of concrete material (E_D), and absorbing energy (E_A), with E_A consisting of elastic and plastic energy that was generated by the pier ($E_{A,P}$), as well as a hysteretic damper or SPDG energy ($E_{A,SPDG}$). The term for Absorbed Energy (E_A) also encompassed the Elastic Strain (E_S) and Plastic (E_{Ps}) Energies arising from the elastic and inelastic reactions of the system, respectively. These energy components were summed up to represent the total amount of energy, as shown in Eq. (14).

$$E_K + E_D + E_{A,P} + E_{A,SPDG} = E_I \tag{14}$$

2.3 Ground motion modeling

The target response spectrum of this study was determined based on AASHTO *Guide Specifications for LFRD Seismic Bridge Design* 2011 (AASHTO 2011), with a 7% probability of exceedance in 75 years. Meanwhile, following ASCE 7-10 (ASCE/SEI 7-10 2013). the nonlinear time history analysis should use at least seven pairs of ground motion records. These records were selected from the ground motion database of the Pacific Earthquake Engineering Research Center (PEER) NGA-West, which was classified as shallow crustal with a strike-slip fault, corresponding to the Opak fault in Yogyakarta. Furthermore, the selection method, which is based on a similar spectral shape to the target response spectrum, was considered as permitted in ASCE 7-10. However, other factors such as the magnitude (M_w), fault distance (R), and site soil class were also considered, although these were not exclusively regarded as the primary selection criteria (ASCE/SEI 7-10 2013). A de-aggregation analysis that combined magnitude and fault distance to the chosen ground motion records in the Yogyakarta region. Specifically, records were selected based on criteria such as magnitude ≥6.5 and fault distance ≤40 km. The soil profile used was classified as site class E, characterized by an average velocity for the upper 30 meters of soil (V_{30}).

An amplitude scaling method was employed for each earthquake record to generate a response spectrum that closely matched the target response spectrum. This method applied a single scale factor as a multiplier to the response spectrum of each earthquake record to enable it to make the average value of the spectral acceleration of each ground motion larger than that of the response spectrum design in a period of interest with ranges from 0.26 s to 1.55 s (Guo *et al.* 2019, Han *et al.* 2019, Darmawan, 2021, Setiawan *et al.* 2021, Santoso *et al.* 2022). Furthermore, the scale factor was calculated according to ASCE 7-10, where SF_x and SF_y denote the scale factors for the longitudinal and transverse directions respectively. The characteristics of the selected ground motion records are presented in Table 4, while the scaled response spectrum is shown in Fig. 8.

3. Result and discussion

3.1 Seismic performance

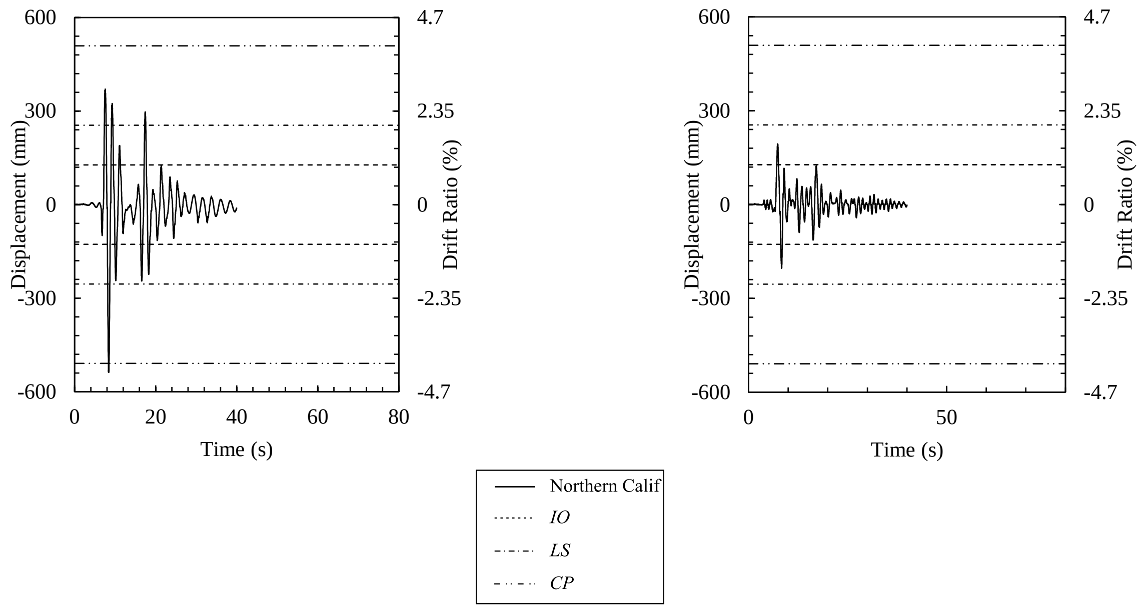

(a) (b)

Fig. 9 Pier displacement in longitudinal direction (a) Model A and (b) Model B

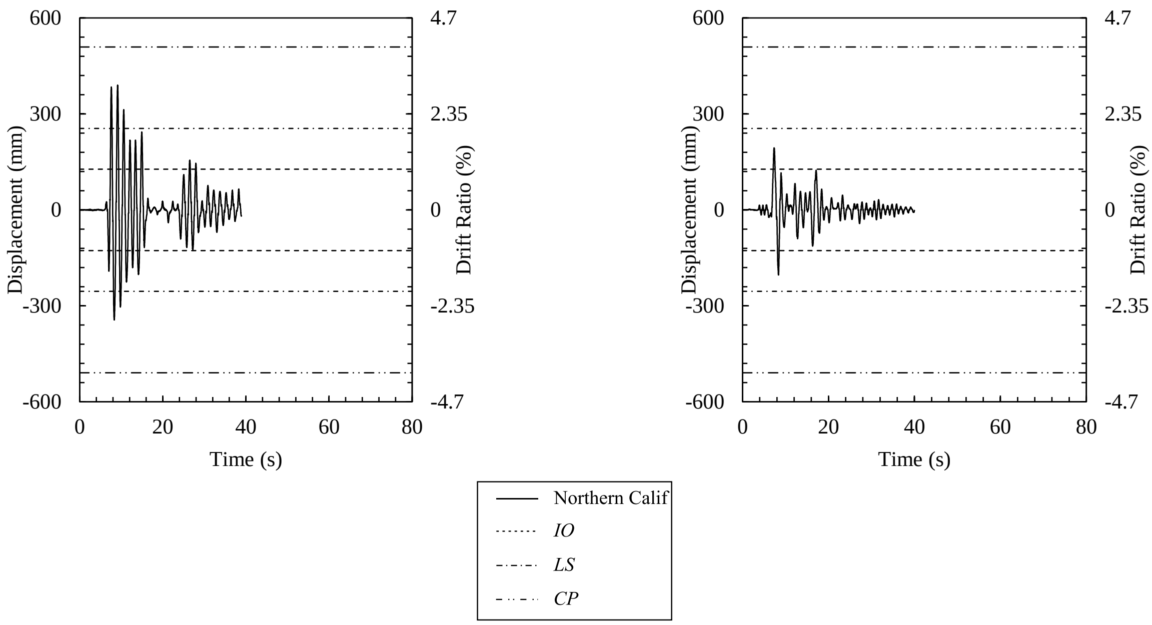

(a) (b)

Fig. 10 Pier displacement in transverse direction (a) Model A and (b) Model B

According to the results obtained from the nonlinear time history analysis, the largest pier response of each model was caused by the Northern Calif Earthquake. In this case, Model A showed a larger top-pier displacement than Model B, as shown in Figs. 9 and 10 respectively. It was observed that Model A resulted in a maximum top pier displacement of 538.11 mm and 419.89 mm in the longitudinal and transverse directions. Meanwhile, Model B showed the maximum top pier displacement of 203.34 mm and 221.39 mm in the longitudinal and transverse directions, respectively. In Model A, during a strong earthquake, the girder deformed until it hit the stopper or shear key that was rigidly bonded to the pier. This caused the pier to move along with the superstructure, resulting in significant displacements (Han *et al*. 2017, Xiang *et al*. 2019). In Model B, after the girder deformation exceeded the gap, the SPDG deformed with a small displacement effect on the pier. This could occur because Model B's horizontal stiffness was only restrained by the ERB and SPDG series, while Model A was fully restrained by the pier.

From the results presented in Tables 5 and 6, it can be observed that the maximum top pier displacements in the longitudinal direction were mostly greater than those in the transverse direction. However, the maximum pier displacement in the transverse direction was not always

Table 5 Pier displacement comparison between Models A and B in a longitudinal direction

No.	Earthquake	Pier displacement in a longitudinal direction				
		Model A (mm)	Performance level	Model B (mm)	Performance level	Reduction (%)
1	Kobe-1104	293.95	*LS*	157.78	*IO*	46.32
2	Darfield	294.69	*LS*	126.50	*IO*	57.07
3	Kobe-1116	122.93	*O*	95.35	*O*	22.43
4	Superstition Hill 02	151.98	*IO*	78.48	*O*	48.37
5	Tottori	177.05	*IO*	121.21	*O*	31.54
6	Northern Calif	538.11	*CP*	203.34	*IO*	62.21
7	Imperial Valley	241.96	*IO*	170.73	*IO*	29.44
	Average	260.09	*LS*	136.20	*IO*	42.48

Table 6 Pier displacement comparison between Models A and B in a transverse direction

No.	Earthquake	Pier displacement in a transverse direction				
		Model A (mm)	Performance level	Model B (mm)	Performance level	Reduction (%)
1	Kobe-1104	399.95	*LS*	221.39	*IO*	46.32
2	Darfield	182.89	*IO*	142.90	*IO*	57.07
3	Kobe-1116	225.54	*IO*	122.71	*O*	22.43
4	Superstition Hill 02	283.06	*LS*	168.11	*IO*	48.37
5	Tottori	221.09	*IO*	135.52	*IO*	31.54
6	Northern Calif	389.63	*LS*	216.67	*IO*	62.21
7	Imperial Valley	419.89	*LS*	190.59	*IO*	29.44
	Average	303.15	*LS*	171.13	*IO*	42.48

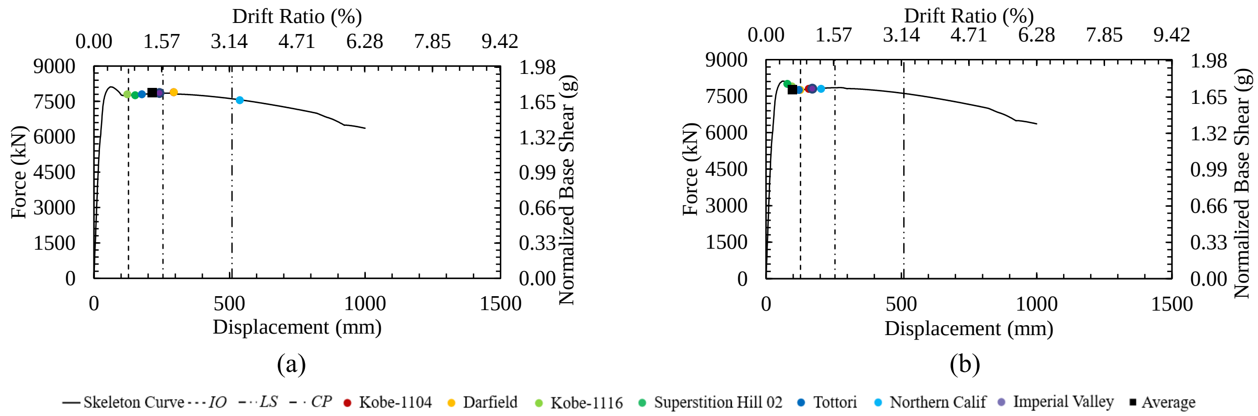

Fig. 11 Pier performance in longitudinal direction (a) Model A and (b) Model B

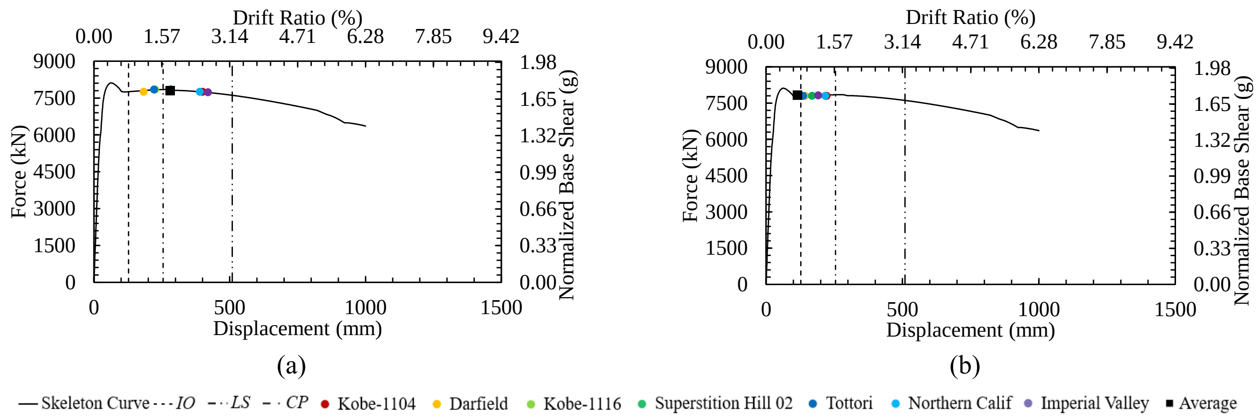

Fig. 12 Pier performance in transverse direction (a) Model A and (b) Model B

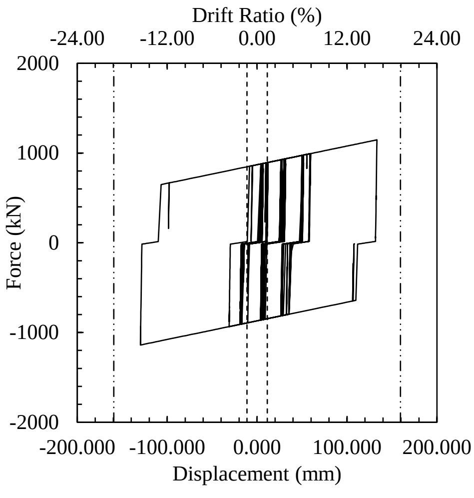

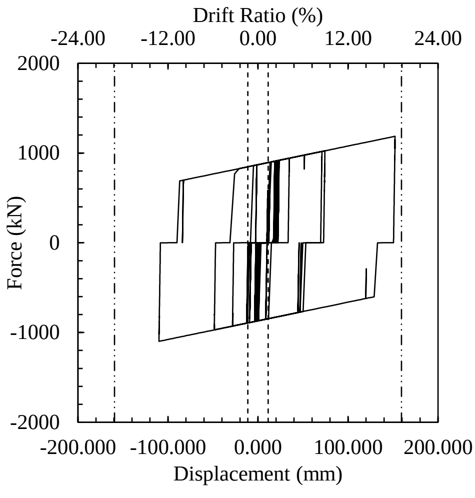

Fig. 13 The SPDG's hysteresis loop (a) Longitudinal direction and (b) Transverse direction

larger than those in the longitudinal direction. Furthermore, the capability of the SPDG to reduce the pier displacement was also measured by dividing the relative pier displacement between Models A and B by that of Model A alone. This process led to the reduction of the average top pier displacement by 42.48% and 41.49% for the longitudinal and transverse earthquakes respectively, indicating that SPDGs are highly capable of reducing pier displacement.

From Figs. 11 and 12, it can be seen that the performance levels of Model B were higher than that of Model A in both the longitudinal and transverse directions. The average performance level of Model A in both directions was classified as *LS*, signifying occurrences of cover concrete spalling and shear cracking in the pier. On the other hand, the average performance level of Model B in both directions was categorized as *IO*, which indicated a minor hairline cracking. This phenomenon showed that several reinforcing steel elements in Model A underwent a more rigorous plastic phase compared to those in Model B. Moreover, the performance level of Model A was spread over the range *O* to *CP*, while for Model B, the performance level was scattered over the range *O* to *LS*. This phenomenon can be attributed to the fact that Model B was equipped with a series of SPDG, which was capable of dissipating the earthquake energy. As a result, Model B demonstrated a better seismic performance level compared to Model A in the longitudinal direction. This result is in line with study conducted by Santoso *et al.* (2023), where it was explained that a box-girder bridge equipped with SPDG had a better seismic performance, achieving a performance level of *O*, whereas the existing bridge without SPDG demonstrated *LS* performance. Likewise, in a study conducted by Haroki *et al.* (2023), it was revealed that the implementation of SPDG significantly enhanced the seismic performance of the slab on a pile bridge. The bridge model equipped with SPDG achieved an *O* performance level, while the performance of the existing bridge without SPDG was categorized as *LS*.

In general, the performance levels in the transverse direction were higher than those in the longitudinal direction, which was evidenced by the obtained pier displacement values of the two models for each ground motion. This phenomenon can be attributed to the fact that, according to the elastic and nonlinear analysis, the longitudinal translation for each model corresponded to mode shape two, while the transverse translation aligned with mode one. Furthermore, although the pier displacement response in transverse directions was higher than those in the longitudinal, the energy reduction in both directions was the same.

Fig. 13 shows the hysteresis loop of a single SPDG resulting from the longitudinal and transverse earthquakes. In this study, it was observed that the SPDGs utilized exhibited an inelastic behavior in response to the designed earthquakes, which was evident from the presence of an energy dissipation phase. Furthermore, the influence of an additional gap can also be observed in Fig. 13, where no strength was exhibited as long as the displacement remained below the gap length of 10 mm. In this state, the ERB functioned to accommodate the movement of the superstructure until the gap length was reached. The yielding state of the SPD occurred subsequently, marking the initiation of inelastic behavior. Analyzing the hysteresis loop, it was evident that the ground motion from Northern California led to the highest shear force experienced by the SPDG compared to the other ground motions. Utilizing this ground motion, the maximum shear force value of 1146.52 kN and 1186.05 kN were observed due to the longitudinal and transverse earthquakes, respectively. Furthermore, the maximum displacement of the SPDG was approximately 133.26 mm and 152.28 mm for the longitudinal and transverse directions. These values were observed to be below the ultimate displacement of SPDG of 159.40 mm, with a drift ratio of 19.20 %. This implies that the SPDG was still able to withstand the designated earthquakes even though it had to be replaced to maintain designated performance. It is crucial to acknowledge that an SPDG displacement value lower than the yield displacement would make the device incapable of dissipating the

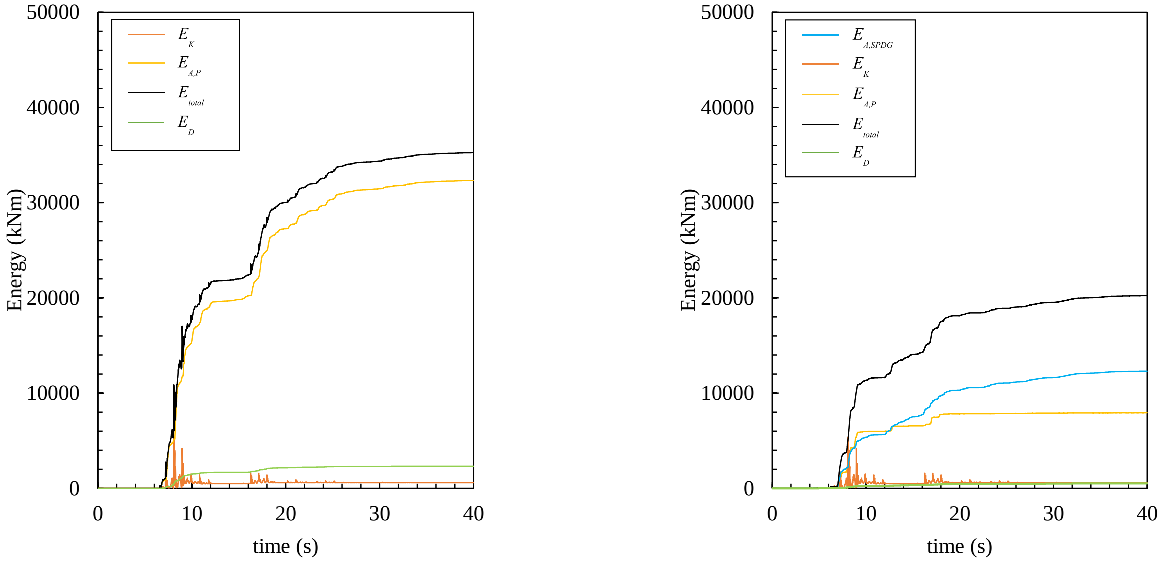

(a) (b)

Fig. 14 Input energy of Northern Calif excitation in longitudinal direction (a) Model A and (b) Model B

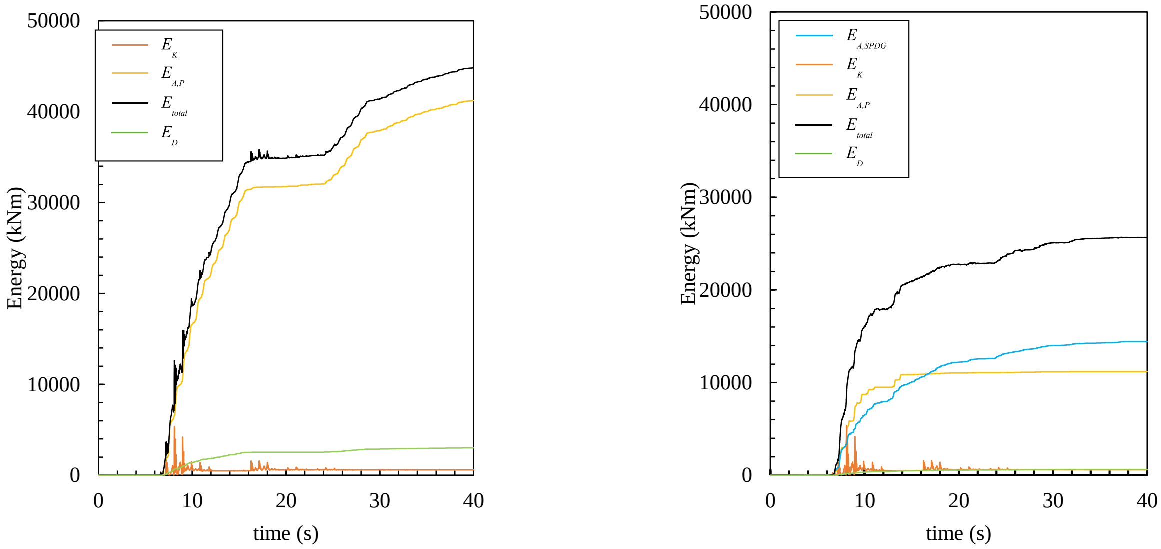

(a) (b)

Fig. 15 Input energy of Northern Calif excitation in transverse direction (a) Model A and (b) Model B

earthquake energy.

3.2 Input energy proportion

The total input energy of Model A was larger than that of Model B. For instance, the northern calif earthquake evoked an input energy of up to 35.91 MNm while that of Model B reached approximately 19.21 MNm, as shown in Figs. 14 and 15. The input energy proportion in Model A was dominated by the pier energy (E_P), which was 25.3 MNm and 32.31 MNm in the longitudinal and transverse directions of earthquakes, respectively. This indicated that the pier received the largest earthquake energy proportion, which resulted in the large earthquake energy absorbed by the plastic hinge. On the other hand, Model B achieved the input energy of 15.44 MNm and 19.21 MNm for the longitudinal and transverse directions, respectively. In this case, the device (E_{SPDG},) provided the largest energy proportion, which was 9.86 MNm and 13.25 MNm for both directions. This implies that a large amount of earthquake energy was absorbed and dissipated by the SPDG instead of the pier. As a result, the pier energy (E_P) of Model B was lower than that of Model A. Besides the smaller pier displacement, the plastic hinge of the two models was compared to each other, and the obtained result indicated that Model A underwent more severe damage than Model B.

In Model A, the proportion of the pier energy to the total energy was 89.66% and 89.97%, while, that of Model B was 42% and 38.92% in the longitudinal and transverse directions respectively. This phenomenon was affected by the larger stiffness of the structural system in Model A, which increased the internal force due to the earthquake excitations (Shen *et al.* 2022). Meanwhile, Model B was accompanied by SPDG, which provided less stiffness between the superstructure and the pier, making the bridge more flexible. This finding is strengthened by a study conducted by Santoso *et al.* (2023), who compared the natural period of the bridge with SPDG and the conventional bridge system with ERB. The result showed that the natural period of the bridge with SPDG was longer than that of the conventional bridge, indicating that the device has the potential of increasing the flexibility of the bridge system. In contrast, this study demonstrated that the inclusion of SPDG effectively dissipated earthquake energy, resulting in a reduction of plastic deformation in the pier and mitigating structural damage.

4. Conclusions

This study investigated the seismic performance enhancement of the PCI-girder bridge using SPDG. Nonlinear time history analysis was performed to determine the behavior of the two bridge models, which were equipped with and without SPDG. Several noteworthy findings emerged from this examination.

The results of the study show that SPDG underwent an inelastic deformation phase, indicating its capability to dissipate earthquake energy. The application of SPDG resulted in notable reductions in both total input energy (EI) and pier energy ($E_{A,P}$) within the bridge system. On the other hand, in the bridge model without SPDG, the proportion of energy concentrated on the pier results in a large proportion of pier energy ($E_{A,P}$). Additionally, SPDG implementation decreased the displacement of the top pier, with reductions of up to 42.48% and 41.49% in longitudinal and transverse directions, respectively. This reduced displacement enhanced the bridge's structural seismic performance from collapse prevention (CP) to immediate occupancy (IO).

SPDG held significant promise for enhancing the seismic performance of PCI-girder bridge systems, which had a large superstructure mass compared to other system. The observed reductions in input energy and bridge structural performance underscored its potential for integration into future bridge designs, contributing to safer and more resilient infrastructure in earthquake-prone regions. It is expedient for further studies to carefully calculate the compatibility of shear strength between SPDG and pier and the ultimate deformation capacity of SPDG in the structural design.

Acknowledgments

The authors are grateful to the Department of Civil and Environmental Engineering at Universitas Gadjah Mada and PT. Raya Consult for the data support, as well as the authors' contribution to this study such as Andika Monanta Emilidardi: data analysis, writing, and editing; Ali Awaludin: conceptualization, review, and editing; Andreas Triwiyono: review; Angga Fajar Setiawan: conceptualization, review, and editing; Iman Satyarno: review.

References

AASHTO (2011), *Guide Specifications for LRFD Seismic Bridge Design*, 2nd Edition, American Association of Highway and Transportation Officials, Washington, D.C., USA.

AASHTO (2017), *LFRD Bridge Design Specifications. Bridge Engineering Handbook: Fundamentals*, 2nd Edition, American Association of Highway and Transportation Officials, Washington, D.C., USA.

Abdel Raheem, S.E. (2009), "Pounding mitigation and unseating prevention at expansion joints of isolated multi-span bridges", *Eng. Struct.*, **31**(10), 2345-2356. https://doi.org/10.1016/j.engstruct.2009.05.010.

ASCE (2000), FEMA 356 Prestandard and Commentary for the Seismic Rehabilitation of Building, Federal Emergency Management Agency, Washington, D.C., USA.

ASCE (2017), Seismic Evaluation and Retrofit of Existing Buildings, Structural Engineering Institute of the American Society of Civil Engineering, Reston, VA, USA.

ASCE/SEI 7-10 (2013), Minimum Design Loads and Associated Criteria for Buildings and Other Structures, Structural Engineering Institute of the American Society of Civil Engineering, Reston, VA, USA.

Becker, T.C. and Mahin, S.A. (2012), "Experimental and analytical study of the bi-directional behavior of the triple friction pendulum isolator", *Earthq. Eng. Struct. Dyn.*, **41**(3), 355-373. https://doi.org/10.1002/eqe.1133.

Bhavani, B.D., Sandhya, K.J. and Manoj, M. (2018), "Analysis of pre-stressed flyover elements", *Int. J. Innov. Res. Sci. Eng. Technol.*, **7**(3), 2917-2923. https://doi.org/10.15680/IJIRSET.2018.0703152.

Bi, K. and Hao, H. (2015), "Modelling of shear keys in bridge structures under seismic loads", *Soil Dyn. Earthq. Eng.*, **74**, 56-68. https://doi.org/10.1016/j.soildyn.2015.03.013.

Bowles, J.E. (1974), *Analytical and Computer Methods in Foundation Engineering*, McGraw-Hill, New York, NY, USA.

BSNI (2016), Perencanaan Jembatan Terhadap Beban Gempa SNI 2833, Badan Standardisasi Nasional Indonesia, Jakarta, Indonesia.

Bukkems, J.M.W. (2017), "Bending-shear interaction of circular hollow sections assessment of the cross-sectional design rules by means of analytical, numerical and statistical evaluation", Master Thesis, Eindhoven University of Technology, Eindhoven, The Netherlands.

Cao, L.Y. and Li, C.X. (2022), "A high performance hybrid passive base-isolated system", *Struct. Control Health Monit.*, **29**(3), e2887. https://doi.org/10.1002/stc.2887.

Chaofeng, Z., Youchun, W., Longfei, W. and Meiping, W. (2017), "Hysteretic mechanical property of low-yield strength shear panel dampers in ultra-large plastic strain", *Eng. Struct.*, **148**, 11-22. https://doi.org/10.1016/j.engstruct.2017.06.028.

Chen, X., De Domenico, D. and LI, C. (2023), "Seismic resilient design of rocking tall bridge piers using inerter-based systems", *Eng. Struct.*, **281**, 115819. https://doi.org/10.1016/j.engstruct.2023.115819.

Chen, Z., Ge, H. and Usami, T. (2006), "Hysteretic model of stiffened shear panel dampers", *J. Struct. Eng.*, **132**(3), 478-483. https://doi.org/10.1061/(asce)0733-9445(2006)132:3(478).

Chen, Z., Ge, H. and Usami, T. (2007), "Study on seismic performance upgrading for steel bridge structures by introducing energy-dissipation members", *J. Struct. Eng.*, **53**, 540-549. https://doi.org/10.11532/structcivil.53A.540.

Darmawan, M.F. (2021), "Pile-supported slab viaduct structure braced with shear panel damper", Master Thesis, Universitas Gadjah Mada, Yogyakarta, Indonesia.

Dindar, A.A., Yalcin, C., Yüksel, E., Ozkaynak, H. and Buyukozturk, O. (2014), "Development of earthquake energy demand spectra", *Earthq. Spectra*, **31**(3), 1667-1689. https://doi.org/10.1193/011212EQS010M.

Filippou, F. and Mazzoni, S. (2012), Steel01 Material, OpenSees, Pacific Earthquake Engineering Research Center, Berkeley, CA, USA. https://opensees.berkeley.edu/wiki/index.php/Steel01_Material

Guo, W., Hu, Y., Liu, H. and Bu, D. (2019), "Seismic performance evaluation of typical piers of China's high-speed railway bridge line using pushover analysis", *Math. Probl. Eng.*, **2019**(1), 9514769. https://doi.org/10.1155/2019/9514769.

Han, Q., Sakata, H., Maida, Y., Mori, T., Maegawa, T. and Zhang, Y. (2019), "Performance evaluation of RC frame with RC wall piers equipped with unbonded steel rod dampers subjected to in-plane loading", *Eng. Struct.*, **197**, 109403. https://doi.org/10.1016/j.engstruct.2019.109403.

Han, Q., Zhou, Y., Ou, Y. and Du, X. (2017), "Seismic behavior of reinforced concrete sacrificial exterior shear keys of highway bridges", *Eng. Struct.*, **139**, 59-70. https://doi.org/10.1016/j.engstruct.2017.02.034.

Haroki, Y., Awaludin, A., Priyosulistyo, H., Setiawan, A.F. and Satyarno, I. (2023), "Seismic performance comparison of simply supported hollow slab on pile group structure with different operational category and shear panel damper application", *Civil Eng. Dimens.*, **25**(1), 10-19. https://doi.org/10.9744/ced.25.1.10-19.

Hube, M.A. and Rubilar, F. (2012), "Capacity evaluation of steel stoppers of reinforced concrete Chilean bridges", *International Symposium for CISMID 25th Anniversary*, Lima, Peru, August.

Jankowski, R., Wilde, K. and Fujino, Y. (2000), "Reduction of pounding effects in elevated bridges during earthquakes", *Earthq. Eng. Struct. Dyn.*, **29**, 195-212. https://doi.org/10.1002/(SICI)1096-9845(200002)29:2%3C195::AID-EQE897%3E3.0.CO;2-3.

Jiang, H., Li, S. and He, L. (2019), "Experimental study on a new damper using combinations of viscoelastic material and low-yield-point steel plates", *Front. Mater.*, **6**, 1-12. https://doi.org/10.3389/fmats.2019.00100.

Kent, D.C. and Park, R. (1971), "Flexural members with confined concrete", *J. Struct. Div.*, **97**(7), 1969-1990. https://doi.org/10.1061/JSDEAG.0002957.

Li, C.X., Pan, H. and Cao, L.Y. (2024), "Pendulum-type tuned tandem mass dampers-inerters for crosswind response control of super-tall buildings", *J. Wind Eng. Indust. Aerodyn.*, **247**, 105706. https://doi.org/10.1016/j.jweia.2024.105706.

Megally, S. (2001), "Seismic response of sacrificial shear keys in bridge abutments", SSRP–2001/23; University of California, San Diego, La Jolla, CA, USA.

Moehle, J.P. and Eberhard, M.O. (2000), *Bridge Engineering Handbook: Earthquake Damage to Bridges*, CRC Press, Boca Raton, FL, USA.

Mohle, J. and Kunnath, S. (2012), Reinforcing Steel Material, OpenSees, Pacific Earthquake Engineering Research Center, Berkeley, CA, USA. https://opensees.berkeley.edu/wiki/index.php/Reinforcing_Steel_Material

Mosalam, K.M., Zareian, F., Taciroglu, E., Omrani, R., Mobasher, B., Liang, X. and Gunay, S. (2015), "Guidelines for nonlinear seismic analysis of ordinary bridges: Version 2.0", CA15-2266, California Department of Transportation, Sacramento, CA, USA.

NCHRP (2013), Performance-Based Seismic Bridge Design: A Synthesis of Highway Practice, Transportation Research Board, Washington, D.C., USA.

Ren, X., Qiang, Z., Dazhu, H. and Dengshan, B. (2021), "Seismic performance study on critically damaged masonry piers retrofitted using shear-compressive metal dampers", *Struct.*, **34**, 3906-3914. https://doi.org/10.1016/j.istruc.2021.10.022.

Sabouri-Ghomi, S., Ventura, C.E. and Kharrazi, M.H. (2005), "Shear analysis and design of ductile steel plate walls", *J. Struct. Eng.*, **131**(6), 878-889. https://doi.org/10.1061/(asce)0733-9445(2005)131:6(878).

Santoso, A.K, Sulistyo, D., Awaludin, A., Fajar Setiawan, A., Satyarno, I., Purnomo, S. and Harry, I. (2022), "Structural systems comparison of simply supported PSC box girder bridge equipped with elastomeric rubber bearing and lead rubber bearing", *Civil Eng. Dimens.*, **24**(1), 19-30. https://doi.org/10.9744/ced.24.1.19-30.

Santoso, A.K., Sulistyo, D., Awaludin, A., Setiawan, A.F., Satyarno, I., Purnomo, S. and Harry, I. (2023), "Comparative study of the seismic performance between simply supported PSC box girder bridge equipped with shear panel damper (SPD) and lead rubber bearing (LRB)", *Int. J. Technol.*, **2024**, 1.

Setiawan, A.F. and Takahashi, Y. (2018), "A high seismic performance concept of integrated bridge pier with triple RC columns accompanied by friction damper plus gap", *J. Japan Soc. Civil Eng. Ser. A1 (Struct. Eng. Earthq. Eng. (SE/EE))*, **74**(4), I_131-I_147. https://doi.org/10.2208/jscejseee.74.i_131.

Setiawan, A.F., Darmawan M.F., Yogatama B.A., Satyarno I. and Guntara M. (2022), "Seismic performance investigation of bracing and SPD application in PHC pile as viaduct piers", *The 17th World Conference on Earthquake Engineering*, Sendai, Japan, September.

Shen, Y., Li, J., Freddi, F., Igarashi, A. and Zhou, J. (2022), "Numerical investigation of transverse steel damper (TSD) seismic system for suspension bridges considering pounding between girder and towers", *Soil Dyn. Earthq. Eng.*, **155**, 107203. https://doi.org/10.1016/j.soildyn.2022.107203.

Shi, G., Gao, Y., Wang, X. and Zhang, Y. (2018), "Mechanical properties and constitutive models of low yield point steels", *Constr. Build. Mater.*, **175**, 570-587. https://doi.org/10.1016/j.conbuildmat.2018.04.219.

Shoaei, P., Tahmasebi Orimi, H. and Zahrai, S.M. (2018), "Seismic reliability-based design of inelastic base-isolated structures with lead-rubber bearing systems, *Soil Dyn. Earthq. Eng.*, **115**, 589-605. https://doi.org/10.1016/j.soildyn.2018.09.033.

Suarjana, M., Octora, D.D. and Riyansyah, M. (2020), "Seismic performance of RC hollow rectangular bridge piers retrofitted by concrete jacketing considering the initial load and interface slip", *J. Eng. Technol. Sci.*, **52**(3), 343-369. https://doi.org/10.5614/j.eng.technol.sci.2020.52.3.4.

Sunardi, B. (2015), "Percepatan tanah sintetis kota Yogyakarta berdasarkan deagregasi Bahaya gempa", *J. Environ. Geol. Hazard.*, **6**(3), 211-228. http://doi.org/10.34126/jlbg.v6i3.85.

Wu, C., Zhang, Q., Huang, W., Zhang, S. and Xu, X. (2022), "Cyclic behavior of metallic damper connected reinforced concrete beam-column joint with an opening in slab", *J. Build. Eng.*, **60**, 105193. https://doi.org/10.1016/j.jobe.2022.105193.

Xiang, N., Alam, M.S. and Li, J. (2019), "Yielding steel dampers as restraining devices to control seismic sliding of laminated rubber bearings for highway bridges: Analytical and experimental study", *J. Bridge Eng.*, **24**(11), 04019103. https://doi.org/10.1061/(ASCE)be.1943-5592.0001487.

Xiang, N., Goto, Y., Alam, M. and Li, J. (2021), "Effect of bonding or unbonding on seismic behavior of bridge elastomeric bearings: Lessons learned from past earthquakes in China and Japan and inspirations for future design", *Adv. Bridge Eng.*, **2**(1), 1-17. https://doi.org/10.1186/s43251-021-00036-9.

Yao, Z., Wang, W. and Zhu, Y. (2021), "Experimental evaluation and numerical simulation of low-yield-point steel shear panel dampers", *Eng. Struct.*, **245**, 1-17. https://doi.org/10.1016/j.engstruct.2021.112860.

Yenidogan, C. (2021), "Earthquake-resilient design of seismically isolated buildings: a review of technology", *Vib.*, **4**, 602-647. https://doi.org/10.3390/vibration4030035.

Yuan, W., Guo, A. and Li, H. (2017), "Seismic failure mode of coastal bridge piers considering the effects of corrosion-induced damage", *Soil Dyn. Earthq. Eng.*, **93**, 135-146. https://doi.org/10.1016/j.soildyn.2016.12.002.

Zhang, C., Aoki, T., Zhang, Q. and Wu, M. (2015), "The performance of low-yield-strength steel shear-panel damper with without buckling", *Mater. Struct. Mater. Constr.*, **48**(4), 1233-1242. https://doi.org/10.1617/s11527-013-0228-9.

Zhang, C., Ding, C., Zhou, Y., Wang, G., Shi, F. and Huang, W. (2023), "Seismic behavior of prefabricated reinforced concrete stair isolated by high damping rubber bearings", *Bull. Earthq. Eng.*, **21**(2), 1325-1352. https://doi.org/10.1007/s10518-022-01548-z.

Zhang, C., Zhang, Z. and Zhang, Q. (2012), "Static and dynamic cyclic performance of a low-yield-strength steel shear panel damper", *J. Constr. Steel Res.*, **79**, 195-203. https://doi.org/10.1016/j.jcsr.2012.07.030.

CC